A HIGHER-ORDER PROJECTION METHOD FOR THE SIMULATION OF UNSTEADY TURBULENT NONPREMIXED COMBUSTION IN AN INDUSTRIAL BURNER

Richard B. Pember, Ann S. Almgren, John B. Bell, Phillip Colella, Louis H. Howell, and Mindy F. Lai
P.O. Box 808, L-316
Lawrence Livermore National Laboratory
Livermore, CA 94550 USA

ABSTRACT

We introduce a new methodology for the modeling of unsteady, nonpremixed, reacting flow in industrial burners which is based on a higher-order projection method for the equations of low-Mach number combustion. The time step used by the method is restricted solely by an advective CFL condition. The method uses standard submodels to account for turbulent transport, kinetics, and radiative transport. The method is presented in the context of axisymmetric flow with swirl in burners with simple boundaries. Numerical results from a sample problem are shown.

INTRODUCTION

We introduce a new methodology for the modeling of unsteady, nonpremixed, reacting flow in industrial burners which is based on a higher-order projection method [1] for the equations of low-Mach number combustion [2]. The method uses explicit, second-order convective differencing but the time step is restricted solely by an advective CFL condition. The methodology is applicable only in the low-Mach number regime ($M < .3$), typically met in industrial burners. Our method is based on an approximate projection formulation [3]. Radiative transport is modeled using the discrete ordinates method [4, 5].

The main goal of this work is to introduce and investigate the simulation of burners using a higher-order projection method for low-Mach number combustion. As such, we only treat the case of axisymmetric flow in gas-fired burners for which the boundaries can be aligned with a rectangular grid, we assume the perfect gas law, and we use several relatively simple, standard submodels, namely, a one-step reduced kinetics mechanism [6], a $k - \epsilon$ model for turbulent transport [7], and a simple turbulent combustion model [8].

Our methodology uses a sequential formulation, and, consequently, compatibility between the continuity equation and the equation of state can-

not be guaranteed [9]. We modify the approach in [1] to account for this.

A number of methodologies for simulating reacting flow are based on SIMPLE [10] and its extensions [11, 12]. Our method is qualitatively similar to SIMPLE in that SIMPLE also uses a sequential formulation with velocity-pressure corrections based on a projection methodology [13]. A projection method for low-Mach number combustion is also presented in [14].

MODEL FOR LOW-MACH NUMBER COMBUSTION

For flow in a spatially open domain the underlying assumption in the low-Mach number model is that M is sufficiently small ($M < .3$) so that the pressure p can be written as the sum of a temporally and spatially constant part p_{amb} and a dynamic part π,

$$p(r,z,t) = p_{amb} + \pi(r,z,t), \tag{1}$$

where $\pi/p_{amb} = O\left(M^2\right)$. The momentum equation can then be written as

$$\rho\left(\frac{DU}{Dt} + G_{acc}(U)\right) = -\nabla\pi + \nabla\cdot\tau, \tag{2}$$

where $U = (u,v,w)^T$ and $G_{acc}(U) = \left(-w^2/r, 0, uw/r\right)^T$. All thermodynamic quantities are considered to be independent of π. The perfect gas law for a multi-component gas in a flow satisfying the low-Mach number assumption is then

$$\rho = p_{amb}/\left(R_{mix}T\right) = p_{amb}/\left(T\mathcal{R}\sum_l \left(m_l/mw_l\right)\right), \tag{3}$$

where $\mathcal{R}$ is the universal gas constant, and m_l and mw_l are the mass fraction and the molecular weight of species l. Differentiating with respect to time,

$$\frac{D\rho}{Dt} = -\rho\left(\frac{1}{T}\frac{DT}{Dt} + \frac{1}{R_{mix}}\frac{DR_{mix}}{Dt}\right)$$

From continuity, $D\rho/Dt = -\rho\nabla\cdot U$ and the following constraint on the divergence of the velocity is obtained:

$$\nabla\cdot U = \frac{1}{T}\frac{DT}{Dt} + \frac{1}{R_{mix}}\frac{DR_{mix}}{Dt} \tag{4}$$

The equations for low-Mach number combustion then consist of (4), (2), and the evolution equations for the other relevant quantities. To close the system of equations, the divergence constraint can be used to derive an elliptic equation for π.

GOVERNING EQUATIONS

The system of governing differential equations consists of the divergence constraint (4), the momentum equation (2), and the following evolution equations for density, temperature, species concentrations, and turbulent kinetic energy and dissipation rate:

$$\frac{\partial \rho}{\partial t} + \nabla \cdot (\rho U) = 0. \tag{5}$$

$$\begin{aligned} \rho c_{p,mix} \frac{DT}{Dt} &= \nabla \cdot ((k + k_t) \nabla T) - \nabla \cdot q_{rad} + H_{fu} R_{fu} \\ &\quad + \nabla \cdot \sum_l \rho h_l(T) (D + D_t) \nabla m_l - \rho \sum_l \frac{Dm_l}{Dt} h_l(T) \end{aligned} \tag{6}$$

$$\frac{\partial (\rho m_l)}{\partial t} + \nabla \cdot (\rho U m_l) = \nabla \cdot ((D + D_t) \rho \nabla m_l) - st_l R_{fu}. \tag{7}$$

$$\rho \frac{Dk}{Dt} = \nabla \cdot \left(\left(\frac{\mu_t}{\sigma_k} + \mu \right) \nabla k \right) - \left(R_{ij} \frac{\partial U_i}{\partial x_j} + \frac{\mu_t}{\rho^2} (\nabla \rho \cdot \nabla p) \right) - \rho \epsilon \tag{8}$$

$$\rho \frac{D\epsilon}{Dt} = \nabla \cdot \left(\left(\frac{\mu_t}{\sigma_\epsilon} + \mu \right) \nabla \epsilon \right) - C_1 \frac{\epsilon}{k} \left(R_{ij} \frac{\partial U_i}{\partial x_j} + \frac{\mu_t}{\rho^2} (\nabla \rho \cdot \nabla p) \right) - C_2 \rho \frac{\epsilon^2}{k} \tag{9}$$

The specific heat of the gas mixture, $c_{p,mix}$, is $\sum_l m_l c_{p,l}(T)$. The stoichiometric ratio st_l is the mass of species l consumed in the reaction per mass of fuel consumed. The stress tensor $\tau = \tau_{lam} - R_{ij}$, where

$$\tau_{lam} = \mu \left(\frac{\partial U_i}{\partial x_j} + \frac{\partial U_j}{\partial x_i} - \frac{2}{3} \delta_{ij} \nabla \cdot U \right), \text{ and}$$

$$-R_{ij} = \mu_t \left(\frac{\partial U_i}{\partial x_j} + \frac{\partial U_j}{\partial x_i} - \frac{2}{3} \delta_{ij} \nabla \cdot U \right) - \frac{2}{3} \delta_{ij} \rho k.$$

The turbulent viscosity, thermal conductivity, and mass diffusivity are defined by

$$\mu_t = C_\mu \rho k^2 / \epsilon, \;\; k_t = c_{p,mix} \mu_t / \sigma_t, \;\; D_t = \mu_t / (\rho \sigma_t)$$

and the standard values of the turbulence model constants [7] are used. The fuel mass consumption rate R_{fu} is the smaller of an Arrhenius reaction rate [6] and an eddy-dissipation rate [8]:

$$R_{fu} = \min \left(\rho^2 m_{fu} m_{ox} A \exp(-E_a / \mathcal{R} T), R_{fu,turb} \right) \tag{10}$$

where

$$R_{fu,turb} = \frac{\epsilon}{k} \min (A' \rho m_{fu}, A' \rho m_{ox} / st_{ox}). \tag{11}$$

We now discuss boundary conditions. The inlet profiles of U, T, and m_l have prescribed values. We use recommended [15, 16] inlet values for k and ϵ,

$$k_{in} = .005 v_{in}^2, \ \epsilon_{in} = C_\mu k_{in}^{3/2}/(.03 D_{in}). \tag{12}$$

At the outflow boundary, the gradients of velocity, temperature, species concentrations, and turbulent quantities are set to zero. At solid walls, the velocity and the gradients of ρ, m_l and k are set to zero. The temperature is a prescribed value. We also use the "law-of-the-wall" [17,16] to compute ϵ, τ, and the conductive heat flux at the wall. The boundary conditions used in computing $\nabla \cdot q_{rad}$ are model-dependent. For the discrete ordinates model, we use the recommendations in [5].

NUMERICAL ALGORITHM

We assume a uniform grid of rectangular cells with widths Δr and Δz indexed by i and j. All quantities in the solution lie on whole time steps (t^n) and are cell-centered with the exception of pressures which lie on cell corners on lagged half-time steps ($t^{n-1/2}$).

The overall strategy of the algorithm in advancing the solution from time t^n to $t^n + \Delta t = t^{n+1}$ is that of a predictor-corrector scheme. In the predictor step, values of $k, \epsilon, w, T, m_l, u$ and v are computed at time t^{n+1}. The values of u and v do not necessarily satisfy the divergence constraint (4). In the corrector step, an elliptic equation is solved to impose this constraint and to update the value of π to $t^n + \Delta t/2$.

The predictor step of the algorithm is itself a multi-step algorithm. A predictor-corrector formulation is used within the predictor step so that second-order accuracy can be obtained. The predictor consists of the following steps:

(1) Compute Δt:

$$\Delta t = \sigma \min_{ij} \left(\frac{\Delta r}{u_{ij}^n}, \frac{\Delta z}{v_{ij}^n} \right) \tag{13}$$

where the CFL number σ satisfies $\sigma < 1$.

(2) Compute values of $u_{i+1/2,j}^{n+1/2}, v_{i+1/2,j}^{n+1/2}$ and $u_{i,j+1/2}^{n+1/2}, v_{i,j+1/2}^{n+1/2}$, at all $r-$ and $z-$ cell edges, respectively, using the higher-order Godunov scheme.

(3) Project edge velocities found in (2) so that they satisfy the divergence constraint.

(4) Compute values of $\varphi_{i+1/2,j}^{n+1/2}$ and $\varphi_{i,j+1/2}^{n+1/2}$ for $\varphi = w$, ρ, ρm_l, T, k, and ϵ using the higher-order Godunov scheme.

(5) Form discrete approximations of convective terms, i.e., $(\nabla \cdot (\rho U \varphi))_{ij}^{n+1/2}$, for $\varphi = 1$, m_l, and $(U \cdot \nabla \varphi)_{ij}^{n+1/2}$ for $\varphi = u$, v, w, T, k, and ϵ.

(6) Compute $\rho_{ij}^{n+1} = \rho_{ij}^{n} + \Delta t \left(\nabla \cdot \rho U\right)_{ij}^{n+1/2}$ and $\rho_{ij}^{n+1/2} = \left(\rho_{ij}^{n} + \rho_{ij}^{n+1}\right)/2$.

(7) Predict values of flow quantities at t^{n+1}, $\varphi_{ij}^{n+1,p}$ for $\varphi = k$, ϵ, m_l, T, u, v, and w, using Crank-Nicholson differencing of the diffusive terms and, for m_l, the reactive terms as well.

(8) Compute $\left(\nabla \cdot q_{rad}\right)_{ij}^{n+1}$ using $T_{ij}^{n+1,p}$.

(9) Compute values of flow quantities, φ_{ij}^{n+1} for $\varphi = k, \epsilon, m_l, T, w$, $u_{ij}^{n+1,*}$, and $v_{ij}^{n+1,*}$, at t^{n+1} using Crank-Nicholson differencing.

In steps (7) and (9) the equations for each of the flow quantities k, ϵ, m_i, T, u, v, and w are solved sequentially in the order listed and the difference equations are formulated so that only linear systems of equations result from the Crank-Nicholson differencing. These linear systems and those arising in the projection steps are solved using the Gauss-Seidel scheme with multigrid acceleration [18].

Numerical Divergence Constraint and Temperature Equation

Several steps in the algorithm require evaluation of $\nabla \cdot U$. The numerical form of the divergence constraint (4) requires modification due to the sequential approach.

The continuity equation (5) and the equation of state (3) are redundant equations for the density ρ. Although the evolution equations with (5) replaced by (3) analytically conserve mass [2], numerical conservation of mass cannot be guaranteed due to the sequential approach used in the predictor step [9]. We therefore use (5) instead of (3).

Using (5), however, makes it necessary to add an extra term to the discrete form of the divergence constraint (4) which accounts for the discrepancy between the values of ρ found by continuity and by the equation of state. The divergence constraint (4) is incremented as follows:

$$\left(\nabla \cdot U\right)_{ij} := \left(\nabla \cdot U\right)_{ij} + f\left(\tilde{p}_{ij} - p_{amb}\right) \frac{c_{p,mix,ij} - R_{mix,ij}}{\Delta t c_{p,mix,ij} \tilde{p}_{ij}} \equiv \tilde{S}_{ij}, \tag{14}$$

where $f = .5$ and $\tilde{p}_{ij} = R_{mix,ij} \rho_{ij} T_{ij}$.

Similarly, the discrete form of the equation for T (6) must be incremented so that it is consistent with (14):

$$\left(\rho c_{p,mix} \frac{DT}{Dt}\right)_{ij} := \left(\rho c_{p,mix} \frac{DT}{Dt}\right)_{ij} - f \frac{\tilde{p}_{ij} - p_{amb}}{\Delta t}. \tag{15}$$

The term $\left(\tilde{p}_{ij} - p_{amb}\right)/\Delta t$ acts to drive the solution back to the constraint $\tilde{p}_{ij} = p_{amb}$. Similar treatments have been used in numerical petroleum reservoir simulation [9].

Predictor

Computation of Edge Velocities at $t^{n+1/2}$. The computation of $(u,v)^{n+1/2}_{i+1/2,j} \equiv U^{n+1/2}_{i+1/2,j}$ and $(u,v)^{n+1/2}_{i,j+1/2} \equiv U^{n+1/2}_{i,j+1/2}$ follows the approach in [19] and consists of two general steps:

(1) The calculation of time-centered left and right edge states, $U^{n+1/2}_{i+1/2,j,L}$ and $U^{n+1/2}_{i+1/2,j,R}$, at all r-cell faces and bottom and top edge states, $U^{n+1/2}_{i,j+1/2,B}$ and $U^{n+1/2}_{i,j+1/2,T}$, at all z-cell faces.

(2) The calculation of time-centered edge states $U^{n+1/2}_{i+1/2,j}$ at all r-cell faces and $U^{n+1/2}_{i,j+1/2}$ at all z-cell faces by an upwinding procedure.

In step (1) cell edge values at $t^{n+1/2}$ are computed using Taylor's theorem and the differential equation (2). For edge $(i+1/2,j)$ this yields

$$\begin{aligned} U^{n+1/2}_{i+1/2,j,L} &= U^n_{ij} + \left(\frac{\Delta x}{2} - \frac{u_{ij}\Delta t}{2}\right) U^n_{x,ij} - \frac{\Delta t}{2}\left(\widehat{vU_y}\right)_{ij} \\ &\quad + \frac{1}{\rho^n_{ij}}\frac{\Delta t}{2}\left(-G_{acc}(U^n_{ij}) - (\nabla\pi)^{n-1/2}_{ij} + (\nabla\cdot\tau)^n_{ij}\right) \end{aligned} \tag{16}$$

and a similar expression for $U^{n+1/2}_{i+1/2,j,R}$. Similar expressions are used to predict values at the other cell edges. Derivatives (e.g., U_x) are evaluated using monotonicity-limited approximations [20]. The computation of the transverse derivative terms (e.g., $\widehat{vU_y}$) and the upwinding procedure follow the approach in [19].

Projection of Normal Edge Velocities. In this step we use a MAC projection [19] to enforce the divergence constraint (14). The equation

$$\left(D^{MAC}\frac{1}{\rho^n}G^{MAC}\phi\right)_{ij} = \left(D^{MAC}U^{n+1/2}\right)_{ij} - \tilde{S}^n_{ij}$$

is solved for ϕ, where $\tilde{S}^n$ is given by (14), and D^{MAC} and G^{MAC} are standard discretizations of the divergence and gradient operators on a staggered grid.

The edge velocities are then corrected by

$$\begin{aligned} u^{n+1/2}_{i+1/2,j} &:= u^{n+1/2}_{i+1/2,j} - \frac{1}{\rho^n_{i+1/2,j}}(G^{MAC}\phi)^r_{i+1/2,j} \\ v^{n+1/2}_{i,j+1/2} &:= v^{n+1/2}_{i,j+1/2} - \frac{1}{\rho^n_{i,j+1/2}}(G^{MAC}\phi)^z_{i,j+1/2}. \end{aligned} \tag{17}$$

Formation of convective derivatives. The values of $\varphi^{n+1/2}_{i+1/2,j}$ and $\varphi^{n+1/2}_{i,j+1/2}$ for $\varphi = w,\ \rho,\ \rho m_l,\ T,\ k$, and ϵ are computed in the same way as the edge values of u, v except that the upwind states are computed using the edge velocities from (17). The discrete approximations to the convective derivatives are then formed using central differences of $\varphi^{n+1/2}_{i+1/2,j}$ and $\varphi^{n+1/2}_{i,j+1/2}$.

Crank-Nicholson Differencing. In steps (7) and (9) of the predictor we solve difference equations obtained by applying the Crank-Nicholson method to the governing equations. In writing the difference equations below, we use ψ to represent all other flow quantities, including $\nabla \cdot U$.

The difference equation for (u, v) is

$$\rho_{ij}^{n+1/2} \left(\begin{array}{l} \dfrac{u_{ij}^{n+1,*} - u_{ij}^{n}}{\Delta t} + ((u,v) \cdot \nabla u)_{ij}^{n+1/2} - \frac{1}{2} \dfrac{\left(w_{ij}^{n+1,p}\right)^2 + \left(w_{ij}^{n}\right)^2}{r_i} \\ \dfrac{v_{ij}^{n+1,*} - v_{ij}^{n}}{\Delta t} + ((u,v) \cdot \nabla v)_{ij}^{n+1/2} \end{array} \right) =$$

$$- (\nabla \pi)_{ij}^{n-1/2} + \frac{L_h\left(u^{n+1,*}, v^{n+1,*}, \psi^{n+1,p}\right) + L_h\left(u^{n}, v^{n}, \psi^{n}\right)}{2}. \qquad (18)$$

where L_h is the discretization of the first two rows of $\nabla \cdot \tau$ in (2).

The difference equations for k, ϵ, T, m_l, and w are similar. The equations for m_l also account for potential stiffness in the R_{fu} term.

In step (7) of the predictor, step n values are used in place of $n+1, p$ values. In step (9), step $n+1$ values of $\varphi = k, \epsilon$, and m_l are used for the predicted values in computing subsequent quantities (e.g., k^{n+1} in computing $\epsilon^{n+1}, u^{n+1,*}$, and $v^{n+1,*}$) in order that proper coupling is obtained. However, consistent values of m_l are used in all approximations of R_{fu}.

Computation of $\nabla \cdot q_{rad}$. We discretize the discrete ordinate equations as conservation relations for each cell [5] and use diamond-difference formulae with flux-limiting. The temperature field $T_{ij}^{n+1,p}$ is used. The system is solved by successive sweeps through the mesh for each ordinate direction. In the computations for this paper we set both reflection and scattering to zero. The ordinate values are taken from the S_6 set listed in [4].

Corrector

In this step, we perform an approximate projection [3] in order to enforce the divergence constraint (14) and find $\pi^{n+1/2}$. In the following, D_a and G_a are standard discretizations of the divergence and the gradient operators. We solve the difference equations

$$\begin{aligned} (L\delta)_{i+1/2,j+1/2} \;=\; & \left(D_a \left(\frac{U^{n+1,*} - U^{n}}{\Delta t} \right) \right)_{i+1/2,j+1/2} - \\ & \frac{\tilde{S}_{i+1/2,j+1/2}^{n+1,p} - \tilde{S}_{i+1/2,j+1/2}^{n}}{\Delta t}, \end{aligned} \qquad (19)$$

where L is a nine-point discretization of $\nabla \cdot (\nabla \delta / \rho)$ based on a finite-element formulation. U_{ij}^{n+1} and $\pi_{i+1/2,j+1/2}^{n+1/2}$ are then computed by

$$U_{ij}^{n+1} = U^{n+1,*} - \frac{1}{\rho_{ij}^{n+1/2}} (G_a \delta)_{ij}\,, \;\; \pi_{i+1/2,j+1/2}^{n+1/2} = \pi_{i+1/2,j+1/2}^{n-1/2} + \delta.$$

NUMERICAL RESULTS

We now discuss results from a simulation of a natural gas-air burner using the above methodology. The following physical properties are as follows. Polynomial curve fits are used for $c_{p,ox}$, $c_{p,pr}$ [21] and $c_{p,fu}$ [22]. Other properties are $A = 10^{10}\text{m}^3/(\text{kg sec})$ and $E_a/\mathcal{R} = 1.84 \times 10^4$ °K [6], $H_{fu} = 4.855 \times 10^7\text{J/kg}$ [21], and $k_a = .2\text{m}^{-1}$. Nominal, constant values of the laminar diffusion coefficients D, k and μ are used.

The geometry of the sample burner is shown in Figure 1. The initial conditions are quiescent and ambient except for a hot spot near the inlet. The inlet conditions are $T_{in} = 300°\text{K}$, $v_{in} = 12.2\text{m/sec}$, no radial velocity, and a tangential velocity profile for the air given by a swirl number of .5 and solid body rotation. The adiabatic flame temperature for our values of T_{in}, c_p and H_{fu} is 2268 °K.

The first two sets of results are for Arrhenius kinetics alone. Figure 2 shows results computed on a 32×128 grid at $t = 1.53$ sec. Temperature, velocity, and air mass fraction are displayed. Figure 3 shows the temperature computed on a 16×64 grid at $t = .075,\ .152,\ .763$, and 1.53 sec. The results at $t = 1.53$ sec for the two resolutions compare favorably, with the coarser grid showing a slightly higher maximum temperature.

Figure 4 shows the effect of the eddy-dissipation model on the temperature field at late time. The results using Arrhenius kinetics alone are included for comparison. The maximum temperatures displayed are 2191°K (Arrhenius kinetics), 2132°K ($A' = 32.0$), and 1780°K ($A' = 4.0$).

DISCUSSION

We have introduced a new methodology for computing time-dependent nonpremixed combustion in burners. The computational results appear reasonable and are consistent under grid refinement. Additional validation is in progress. The turbulent combustion model also warrants further investigation.

We are uncertain as to why the computations discussed in the previous section effectively reached steady state after the unreasonably short simulated time of 1.53 sec. One possible explanation is that buoyancy effects are neglected. A second is that rapid attainment of steady state conditions may be an artifact of the $k - \epsilon$ model.

There are several areas of further research in this methodology being pursued by the authors. In addition to continuing validation of the method, we are extending it to more complex geometries. We plan to extend it to three spatial dimensions, as well as incorporate more sophisticated turbulence and

kinetics models.

Acknowledgements

The above work was performed under the auspices of the U.S. Department of Energy by the Lawrence Livermore National Laboratory under contract W-7405-Eng-48. Support under this contract was provided by the Applied Mathematical Sciences Program and the HPCC Grand Challenge Program of the Office of Scientific Computing at DOE. Dr. Colella was also partially supported by DARPA and the National Science Foundation under grant DMS-8919074; and by a National Science Foundation Presidential Young Investigator award under grant ACS-8958522; and by the Department of Energy HPPC Program under grant DE-FGO3-92ER25140.

We would like to thank Steve Londerville and Scott Drenan of Coen Company, Inc., for a number of helpful discussions during the course of this research.

REFERENCES

1. M. Lai, J.B. Bell, and P. Colella, "A Projection Method for Combustion in the Zero Mach Number Limit", *Proceedings, AIAA 11nd Computational Fluid Dynamics Conference, Orlando, FL*, July 6-9, 1993, p.776-783, AIAA Paper 93-3369-CP.

2. A. Majda and J.A. Sethian, "The Derivation and Numerical Solution of the Equations for Zero Mach Number Combustion", *Combust. Sci. Tech.*, vol. 185-205, pp. 185-205, 1985.

3. A.S. Almgren, J.B. Bell, and W.G. Szymczak, "A Numerical Method for the Incompressible Navier-Stokes Equations Based on an Approximate Projection", UCRL-JC-112842, Lawrence Livermore National Laboratory, January, 1993, *SIAM J. Sci. Comput*, accepted for publication.

4. W. A. Fiveland, "Discrete-Ordinates Solutions of the Radiative Transport Equation for Rectangular Enclosures", *J. Heat Transfer*, vol. 106, pp. 699–706, 1984.

5. E. E. Lewis and W.F. Miller, Jr., *Computational Methods of Neutron Transport*, American Nuclear Society, La Grange Park, IL, 1993.

6. E.E. Khalil, D.B. Spalding, and J.H. Whitelaw, "The Calculation of Local Flow Properties in Two-Dimensional Furnaces", *Int. J. Heat and Mass Transfer*, vol. 18, pp. 775-791, 1975.

7. W.P. Jones and J.H. Whitelaw, "Modeling and Measurements in Turbulent Combustion", *Twentieth Symposium (International) on Combustion*, pp. 233-249, The Combustion Institute, 1984.

8. R.W. Bilger, "Turbulent Diffusion Flames", *Ann. Rev. Fluid Mech.*, vol. 21, pp. 101-135, 1989.

9. J.A. Trangenstein and J.B. Bell, "Mathematical Structure of the Black-oil Model for Petroleum Reservoir Simulation", *SIAM J. Appl. Math.*, vol. 49, pp. 749-783, 1989.

10. L.S. Caretto, A.D. Gosman, S.V. Patankar, and D.B. Spalding, "Two Calculation Procedures for Steady, Three-Dimensional Flows with Recirculation", *Proceedings of the Third International Conference on Numerical Methods in Fluid Mechanics*, Paris, France, July, 1972, Vol. II, pp.60-68.

11. P.A. Gillis and P.J. Smith, "An Evaluation of Three-Dimensional Computational Com-

bustion and Fluid Dynamics for Industrial Furnace Geometries", *Twenty-Third Symposium (International) on Combustion*, pp. 981-991, The Combustion Institute, 1990.
12. Khalil, E.E, *Modeling of Furnaces and Combustors*, Abacus Press, 1982.
13. F. Harlow and J. Welch, "Numerical Calculation of Time-dependent Viscous Incompressible Flow of Fluids with Free Surfaces", *Phys.Fl.*, vol. 8, pp. 2182-2189, 1964.
14. H. Dwyer, "Calculation of Low Mach Number Reacting Flows", *AIAA Journal*, vol. 28, pp. 98-105, 1990.
15. A.D. Gosman, F.C. Lockwood, and A.P. Salooja, "The Prediction of Cylindrical Furnaces Gaseous Fueled with Premixed and Diffusion Burners", *Seventeenth Symposium (International) on Combustion*, pp. 747-760, The Combustion Institute, 1978.
16. D.G. Sloan, P.J. Smith, and L.D. Smoot, "Modeling of Swirl in Turbulent Flow Systems", *Prog. Energy Combust. Sci.*, vol. 12, pp. 163-250, 1986.
17. B.E. Launder and D.B. Spalding, "The Numerical Computation of Turbulent Flows", *Comp. Meth. Appl. Mech. Eng.*, vol. 3, pp. 269-289, 1974.
18. W.L. Briggs, *A Multigrid Tutorial*, SIAM, Philadelphia, PA, 1987
19. J. B. Bell and P. Colella and L. H. Howell, "An Efficient Second-Order Projection Method for Viscous Incompressible Flow", *10th AIAA Computational Fluid Dynamics Conference*, Honolulu, June 24–27, 1991.
20. P. Colella, "A Direct Eulerian MUSCL Scheme for Gas Dynamics", *SIAM J. Sci. Stat. Comput.*, vol. 6, pp. 104-117, 1985.
21. R.J. Tucker and J.M. Rhine, *Modelling of Gas-Fired Furnaces and Boilers*, British Gas, McGraw-Hill, 1991.
22. S. Glasstone, *Thermodynamics for Chemists*, van Nostrand Co., Princeton, 1947.

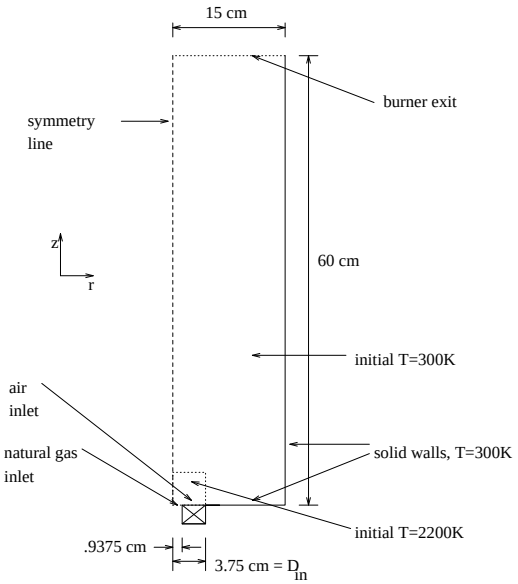

Figure 1: Configuration of burner for sample problem.